

Diamond-based electron emission: Structure, properties and mechanisms

Liang-Xue Gu(顾梁雪), Kai Yang(杨凯), Yan Teng(滕妍), Wei-Kang Zhao(赵伟康), Geng-You Zhao(赵耕右), Kang-Kang Fan(凡康康), Bo Feng(冯博), Rong Zhang(张荣), You-Dou Zheng(郑有炓), Jian-Dong Ye(叶建东), Shun-Ming Zhu(朱顺明), Kun Tang(汤琨), and Shu-Lin Gu(顾书林)

Citation: Chin. Phys. B, 2024, 33 (**9**): 098102. DOI: 10.1088/1674-1056/ad5aec
Journal homepage: http://cpb.iphy.ac.cn; http://iopscience.iop.org/cpb

What follows is a list of articles you may be interested in

Synthesis and nitrogen content regulation of diamond in a high-pressure hydrogen-rich environment

Guofeng Huang(黄国锋), Liangchao Chen(陈良超), and Chao Fang(房超)
Chin. Phys. B, 2024, 33 (**6**): 068102. DOI: 10.1088/1674-1056/ad2a6d

Diamond growth in a high temperature and high pressure Fe-Ni-C-Si system: Effect of synthesis pressure

Yang Liu(刘杨), Zhiwen Wang(王志文), Bowei Li(李博维), Hongyu Zhao(赵洪宇), Shengxue Wang(王胜学), Liangchao Chen(陈良超), Hongan Ma(马红安), and Xiaopeng Jia(贾晓鹏)
Chin. Phys. B, 2023, 32 (**12**): 128102. DOI: 10.1088/1674-1056/acf03d

Effects of oxygen/nitrogen co-incorporation on regulation of growth and properties of boron-doped diamond films

Dong-Yang Liu(刘东阳), Kun Tang(汤琨), Shun-Ming Zhu(朱顺明), Rong Zhang(张荣), You-Dou Zheng(郑有炓), and Shu-Lin Gu(顾书林)
Chin. Phys. B, 2023, 32 (**11**): 118102. DOI: 10.1088/1674-1056/ace4b7

High performance trench diamond junction barrier Schottky diode with a sidewall-enhanced structure

Ying Zhu(朱盈), Wang Lin(林旺), Dong-Shuai Li(李东帅), Liu-An Li(李柳暗), Xian-Yi Lv(吕宪义), Qi-Liang Wang(王启亮), and Guang-Tian Zou(邹广田)
Chin. Phys. B, 2023, 32 (**8**): 088101. DOI: 10.1088/1674-1056/acc2ae

Determination of band alignment between GaO_x and boron doped diamond for a selective-area-doped termination structure

Qi-Liang Wang(王启亮), Shi-Yang Fu(付诗洋), Si-Han He(何思翰), Hai-Bo Zhang(张海波),Shao-Heng Cheng(成绍恒), Liu-An Li(李柳暗), and Hong-Dong Li(李红东)
Chin. Phys. B, 2022, 31 (**8**): 088104. DOI: 10.1088/1674-1056/ac464e

---

REVIEW

Diamond-based electron emission: Structure, properties and mechanisms

Liang-Xue Gu(顾梁雪), Kai Yang(杨凯), Yan Teng(滕妍), Wei-Kang Zhao(赵伟康), Geng-You Zhao(赵耕右), Kang-Kang Fan(凡康康), Bo Feng(冯博), Rong Zhang(张荣), You-Dou Zheng(郑有炓), Jian-Dong Ye(叶建东), Shun-Ming Zhu(朱顺明), Kun Tang(汤琨)[†], and Shu-Lin Gu(顾书林)[‡]

School of Electronic Science and Engineering, Nanjing University, Nanjing 210046, *China*

(Received 11 April 2024; revised manuscript received 6 June 2024; accepted manuscript online 24 June 2024)

Diamond has an ultrawide bandgap with excellent physical properties, such as high critical electric field, excellent thermal conductivity, high carrier mobility, etc. Diamond with a hydrogen-terminated (H-terminated) surface has a negative electron affinity (NEA) and can easily produce surface electrons from valence or trapped electrons via optical absorption, thermal heating energy or carrier transport in a PN junction. The NEA of the H-terminated surface enables surface electrons to emit with high efficiency into the vacuum without encountering additional barriers and promotes further development and application of diamond-based emitting devices. This article reviews the electron emission properties of H-terminated diamond surfaces exhibiting NEA characteristics. The electron emission is induced by different physical mechanisms. Recent advancements in electron-emitting devices based on diamond are also summarized. Finally, the current challenges and future development opportunities are discussed to further develop the relevant applications of diamond-based electron-emitting devices.

Keywords: diamond, negative electron affinity (NEA), PN junction, electron emission

PACS: 81.15.Gh, 81.05.ug, 07.30.Bx, 07.30.Kf **DOI:** 10.1088/1674-1056/ad5aec

1. Introduction

Diamond possesses a high refractive index and low absorption coefficient for visible light, and is transparent in most infrared and ultraviolet regions. It holds potential application value in the fields of optoelectronics, such as visible intraocular lenses, x-ray refractive lenses and spectrometers.[1] Furthermore, it exhibits the highest thermal conductivity among all known substances, with a maximum value of 1.5×10^5 W·m^{-1}·K^{-1} at 80 K, making it a crucial material for heat sinks. When in direct contact with an electronic chip, it can rapidly transfer heat out of the circuit, ensuring smooth device operation.[2] In addition, with its remarkable mechanical properties and extremely low dielectric losses, diamond stands as the only material suitable for the power transmission window in the gyrotron of a fusion reactor.[3,4]

With a face-centered cubic structure, the carbon atoms in diamond are grouped through sp^3 hybrid orbitals at the vertices of regular tetrahedra, establishing covalent C–C bonds with neighboring carbon atoms to produce an endless three-dimensional structure (Fig. 1(a)).[5–7] It also has three crystal planes (111), (100) and (110), and its common crystal shapes are primarily tetrahedron and octahedron. In addition, the C–C bond formed in the diamond has a short bond length ($\sim$ 154.45 pm) and a large bond energy ($\sim$ 347.5 kJ·mol^{-1}). Therefore, the Young's modulus, tensile strength and thermal expansion coefficient are the highest among solid materials in nature.[8,9] The arrangement of C atoms is also symmetrical and all the valence electrons are involved in bonding, which is the reason for no freely moving electrons in diamond.[5] Doping can improve the conductivity of diamond, which is initially akin to that of an insulator.[10–12] For example, the introduction of boron (B) as a dopant can produce acceptor characteristics that are conducive to conductivity at room temperature (RT). Phosphorus-doped (P-doped) n-type diamond possesses a deeper electron donor energy level, but the doped material is only effective at elevated temperatures. In contrast, nitrogen-doped (N-doped) diamond creates nitrogen vacancy (NV) center defects. This is frequently employed in areas such as sensing and energy-related technologies,[13] optoelectronic and quantum computer engineering[14] and interference-free GPS navigation exploration.[15] More importantly, the diamond surface combined with hydrogen terminals exhibits significant negative electron affinity (NEA), facilitating electron emission. Its unique physical properties make it valuable in various electron-emitting devices, such as spacecraft ion engines and electron microscopes.[16] Studies have shown that combining diamond with other substances enhances field-emission efficiency, lowering the turn-on electric field value and increasing the field enhancement factor.[17] Diamond's NEA reduces electron emission barriers, protecting the emitter from ion bombardment and extending its service life.[18]

[†]Corresponding author. E-mail: ktang@nju.edu.cn
[‡]Corresponding author. E-mail: slgu@nju.edu.cn

© 2024 Chinese Physical Society and IOP Publishing Ltd

Moreover, the charge collection efficiency in diamond PIN diodes reaches 98%, which is comparable to traditional silicon photodiodes and is highly anticipated in power electronic devices with ultra-high blocking voltages.[19]

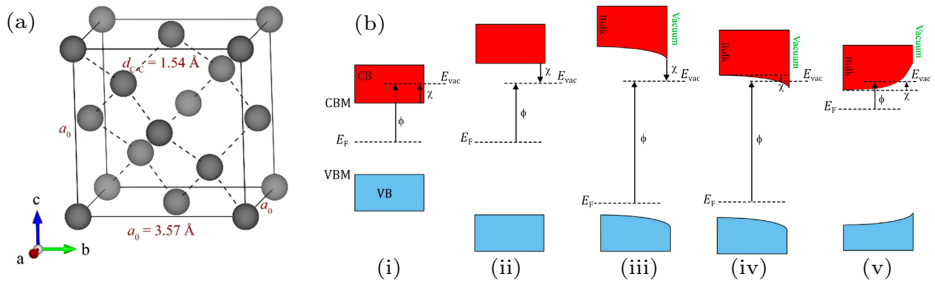


Fig. 1. (a) Crystal structure of diamond.[20] (b) Electron affinity of semiconductors and its relationship with work function and fixed vacuum energy level.[16] VB represents the valence band, VBM is its maximum energy, CB represents the conduction band and CBM is its minimum energy.

The conduction band (CB) of conventional semiconductors usually lacks electrons, while the valence band is mostly filled. The Fermi level (E_F) is positioned between the top of the valence band and the bottom of the conduction band, resulting in a positive electron affinity (PEA) (Fig. 1(b)(i)).[16,21] When the conduction band energy level exceeds the vacuum level, a negative electron affinity is observed, mainly in wide bandgap materials such as diamond (Fig. 1(b)(ii)). Band bending occurs due to charge distribution imbalance at the interface. In p-type doped materials, the Fermi level stays close to the valence band maximum, lowering both the conduction band and valence band at the surface. The conduction band minimum still exceeds the vacuum level, maintaining NEA (Fig. 1(b)(iii)). However, if the new conduction band minimum induced by band bending falls below the vacuum level, a different scenario is observed in Fig. 1(b)(iv). In n-type semiconductors, the energy bands bend upwards, with the Fermi level near the top of the band gap, approaching the bulk conduction band minimum (Fig. 1(b)(v)).[21,22] This arrangement results in a reduced work function. N-doped materials are excellent for enhancing electron emission and the C–H bonds on the surface of n-doped diamond exhibit negative electronegativity, leading to the surface being enriched with numerous electrons, while many holes accumulate in the subsurface. On the other hand, surface states appear at the valence band edge of the hydrogen-terminated surface, inducing band bending upwards by pinning the Fermi level. However, this can lead to positive electron affinity due to the upward band bend. Conversely, in p-type materials with a noticeable downward band bend, less energy is needed to excite and emit electrons.[23,24]

Diamond's low work function surface resulting from the combination of the donor state and NEA significantly reduces the emission barrier for electrons, reduces electron power consumption and accelerates emission speed.[25] Hence, it is suitable for electron emission applications.[26] Due to the strong covalent bonding of C–H, the hydrogen-terminated (H-terminated) diamond surfaces naturally exhibit NEA in a vacuum with very high thermal and chemical stability. The surface remains stable even after exposure to air or heating to over 400 °C.[27] However, the CBM only contains a small number of electrons. Therefore, injecting electrons into the diamond CB is a crucial technology for utilizing the NEA surface for electron emission.[28] Applying an electric field to the NEA surface can reduce the internal potential barrier, and electrons in the conduction band are emitted from the surface to the vacuum.[29–31] The electrons are located in the CB, so n-type P-doped diamond will also emit electrons.[32] The electron emission of P-doped diamond film at low threshold voltage is very limited,[33] but the surface of the diamond film will also show relatively stable emission after modification.[29,34] The ion implantation process is another effective means to enhance the electron emission performance and help improve the conductivity of diamond films.[35–39] Beyond that, other factors such as grain morphology,[40–43] substrate material, conductivity and surface treatment methods will also affect the final electron emission state of diamond.[37,44]

In this review, we will analyze the fundamental configuration of diamonds, encompassing the energy band and the PN junction structure. In addition, we concentrate on the significant advancements in diamond regarding various electron emission mechanisms, such as field electron emission, photoelectron emission and thermal electron emission. Furthermore, we elaborate on the potential applications of diamond films with favorable electron emission characteristics in the realm of electron sources. Finally, we present the challenges and potential future paths to address issues related to diamond devices, along with suggesting strategies for resolution.

2. Diamond PN junction

The Schottky PN diode represents a unique power device with the ability to independently control blocking voltage and on-resistance.[45] The diamond PN structure facilitates electron injection,[46] presenting a new opportunity for creating efficient electron emitters.

2.1. Diamond PN junction

In 2001, Koizumi achieved the successful preparation of a B and P-doped diamond PN junction through epitaxial growth on a single-crystal diamond substrate. The device demonstrated clear diode characteristics and exhibited the emission of ultraviolet light with a wavelength of 235 nm.[47] Under forward bias, electron emission was observed when the diode was conducted, with the emission becoming more pronounced as the forward diode current increased. Conversely, no electron emission was observed under reverse bias, confirming that electron emission is driven by electron injection at the PN junction interface.[48] The PN junction demonstrates rectifying diode characteristics, and electron emission from the p-type layer is observed when the diode is in forward biased state. The initial device displayed an electron emission efficiency of 0.64%, and this was later enhanced to 1.4% through improvements in the crystal quality of the semiconductor diamond layer.[49]

In Fig. 2(a), the current of electron emission is observed within the H-terminated PN junction diamond diode, and the electrons in the N layer migrate towards the P layer under forward bias, which are detected from the NEA diamond surface through the total photoelectron yield spectrum, leading to exciton-derived photoelectron emission.[50] This phenomenon is attributed to exciton diffusion under forward bias (Fig. 2(b)).[51,52] In Fig. 2(c), it is evident that electron emission is positively correlated with forward diode current. Significant leakage current is also observed, but no electron emission is observed under reverse bias. This confirms that electron emission is driven by electron injection at the PN junction interface. When electrons are injected from the n-type layer, they will move in the conduction band of p-type diamond and fill empty surface states on the hydrogen-terminated surface. If the energy of these electrons exceeds the vacuum energy level, some of them will be released into the vacuum.[49]

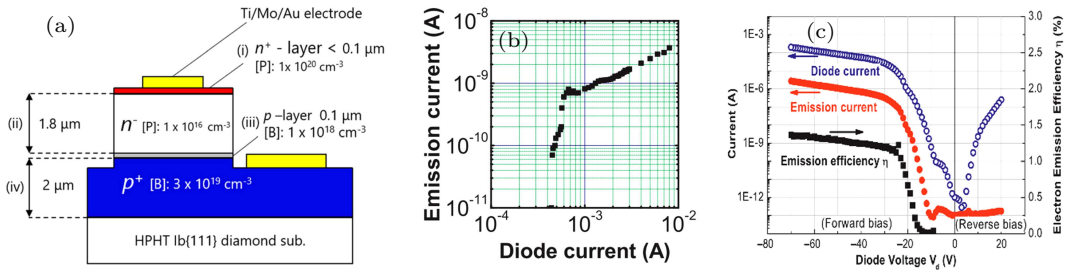


Fig. 2. (a) Schematic diagram of diamond PN diode.[50] (b) Emission current of diamond (001) PN junction diode.[51] (c) Electron emission and diode characteristics of diamond PN junction cathodes.[49]

2.2. Diamond PIN junction

The deep level of P donors in n-type diamond needs to be activated at temperatures between 200 °C and 300 °C,[52] which is a primary challenge limiting the operation of diamond electron emitters at RT. Furthermore, the higher the current, the higher the electron emission derived from excitons, combining the strong binding energy of free excitons and the small Bohr radius with the result that PIN junctions are more suitable for enhancing excitonic properties than PN junctions and function as an indirect transition semiconductor. A high-quality thick intrinsic layer (I-layer) can increase the radiative recombination surface area of free excitons.[53,54] A heavily P-doped N^+ top layer reduces the series resistance and increases the net current of the diode.[30,55] Increasing the doped donor concentration reduces the series resistance of the PIN junction, allowing higher current injection and maintaining lower temperatures.[56–58] Furthermore, the high-level doping significantly decreases contact resistance, whereas low-level doping enhances carrier lifetime and mobility in the active layer of the junction devices.[62–69]

The I-layer in the PIN structure contains a high density of free excitons, providing clear advantages.[56,65] Carriers or excitons injected into the I-layer have a broad distribution area and a relatively long lifetime. Thus, a thicker I-layer with a similar carrier distribution area is expected to achieve higher emission efficiency.[55] Undoped I-layer is grown as a PIN junction of the active layer, achieving stronger exciton emission intensity. The I-layer sandwiched between the P-layer and N-layer supports high reverse blocking voltage. The highest breakdown voltage of 11.5 kV was reported as having been achieved using a PIN structure.[66]

Tatsuya *et al.* fabricated PIN diodes with high ($B = 10^{20}$ cm^{-3}) and low ($B = 2 \sim 4 \times 10^{18}$ cm^{-3}) B doping, respectively.[63] As can be seen in Figs. 3(a) and 3(b), upon increasing the bias voltage, both the diodes' I_d and I_e show significant increase from the built-in potential of 4.5 V, suggesting that upon diode activation, electrons within the diamond are emitted into the vacuum under the influence of NEA. In the case of PIN^+ diodes, the electron emission efficiency also rises with increasing forward bias voltage. However, for $P^{++}IN^+$ diodes, the electron emission efficiency declines when the forward bias voltage exceeds approximately 10 V. In the I_d dependence diagram of the electron emission efficiency, the maximum forward current level is limited to 4×10^{-3} A for PIN^+

diodes and 10^{-1} A for $P^{++}IN^{+}$ diodes. This confirms that the electron emission efficiency of heavily doped samples is 2–3 orders of magnitude inferior to that of lightly doped PIN^{+} diodes.[63] It is shown in Figs. 3(c) and 3(d) that under the forward bias of the PIN diode, the current increases to 400 mA and the electron emission current exceeds 7 μA.[64]

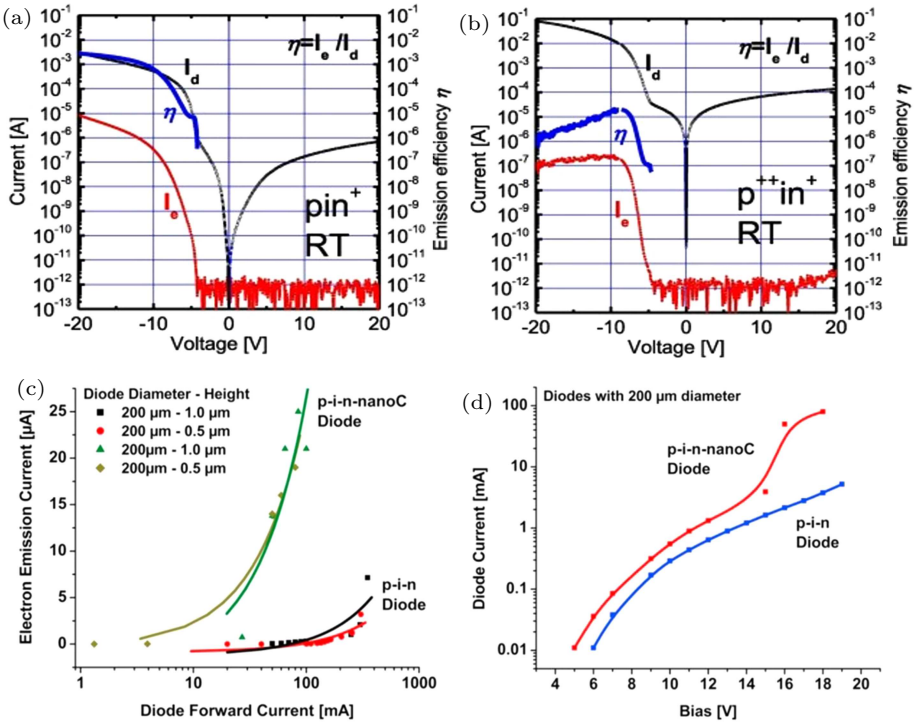


Fig. 3. (a) PIN^{+}, $P^{++}IN^{+}$ dependence of diode current I_d and emission current I_e on applied voltage and I_d dependence of electron emission efficiency.[63] (b) Electron emission of diamond PIN, PIN-nanoC diode.[64]

Takeuchi *et al.* fabricated PIN diodes[62,67] and found that the "excited state" of the diamond diode induced electron emission and photoelectron excitation, with electron emission ultimately observed exclusively in the hydrogenated device. The higher the diode current (I_d), the longer the free exciton lifetime, demonstrating that the short lifetime issue is addressed through deep recombination of indirect semiconductor properties, $\eta = 0.2\%$ was achieved in RT experiments, while no electron emission was observed before hydrogenation, suggesting that electron emission is the result of NEA on the diamond surface. In addition, no I_e was observed in the reverse-biased region in the relationship between the obtained η and I_d, and it is believed that the apparent "excited" state of the diamond diode with forward current is what triggers electron emission and photoelectron excitation. It is shown that electrons injected from the N layer to the I layer contribute to electron emission and exciton-derived electron emission may be associated with high current injection regions.[62,67]

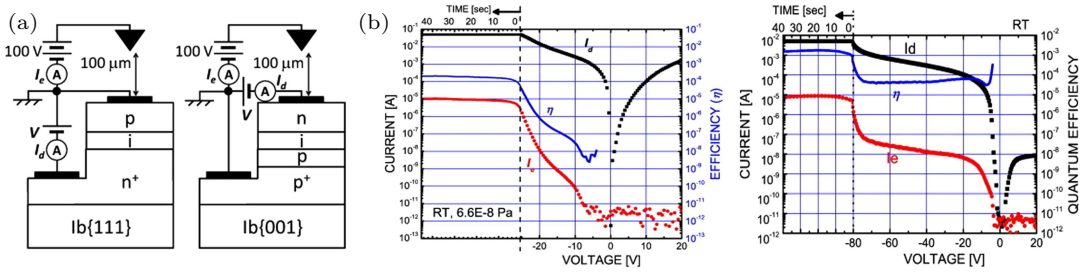


Fig. 4. (a) Schematic diagrams of different diode structures. (b) Relationship between the forward current of different diodes and the voltage applied to the diode.[68]

In Fig. 4(a), when the NIP junction is on the P top layer, as the bias voltage increases from −20 V to +4 V, the capacitance gradually increases, indicating the presence of a space charge layer that extends to the P and N layers, and becomes narrower as the bias voltage increases.[68] Figure 4(b) illustrates the NIP^{+} and PIN^{+} diodes and the current–voltage dependency of diode emission. Before hydrogenation, there was no observed electron emission, demonstrating that the diode emission is correlated with the NEA of the diamond surface. Following hydrogenation, electron emission began to be ob-

served under forward bias. The diode utilizes an N^+ layer, which significantly reduces contact resistance. Hence, the observed emission threshold voltage is nearly the same as the expected built-in potential. Overall, the emission process begins when the applied bias voltage creates flat-band conditions, and *C*–*V* tests demonstrate carrier injection into the I-layer. Both diodes show an increase in efficiency and a non-linear increase in emission current as the diode current rises. This indicates that the efficiency of the electron emission mechanism depends on the diode current level rather than the conduction type at the top of the high current injection region.

3. Diamond-based electron emission

The exceptional physical properties of diamonds hold significant potential for electron-emitting devices, and the formed NEA surface is frequently employed in electron emission research. Depending on the different physical mechanisms of induced electron emission, it can be categorized into photoelectron, thermal electron and field electron emission.[69] At times, the electron emission modes are combined to achieve optimal device performance.[70]

3.1. Field-induced electron emission

Field electron emission (FE) primarily functions to mitigate the surface barrier of an object by imposing an external electric field. This reduces the height and narrows the width of the surface barrier, facilitating electron penetration and an escape through the tunnel effect. The key targets for optimizing FE are achieving high emission current and low operating voltage.[71–73] The reduction in operating voltage is achieved through field enhancement and emission microstructure optimization, involving the creation of whiskers,[74] pyramids[75] and cones[76] on the diamond surface. The formation of sharp protrusions on the diamond surface is expected to enhance the electric field, allowing the extraction of electrons at lower electric fields. Another approach involves the utilization of diamond semiconductors with NEA.[77,78] For instance, the vertically aligned diamond sample fabricated by Zhang *et al*. demonstrated outstanding FE characteristics with a low turn-on field and a high emission current density.[79]

Figure 5(a) displays the spectral responsivity of microcrystalline diamond (MCD), sub-microcrystalline diamond (SMCD) and nanocrystalline diamond (NCD) in the FE configuration.[80] Region A corresponds to a direct inter-band transition within the diamond band gap (5.6 eV), which decreases in SMCD and NCD due to the increase in the mid-bandgap state. Region B corresponds to the transition from the valence band to the mid-bandgap state 0.5–0.7 eV below the conduction band and is associated with point defects, sulfur doping and grain boundaries.[84] These transitions are enhanced in SMCD and NCD, increasing the responsivity in the B region. Region C is related to the NEA of diamond, wherein the termination of H in diamond forms heteropolar C–H bonds, generating negatively charged H (surface side) and positively charged C (film side), which reduces the work function of the material.[80,85] Figure 5(b) shows that UPS without applied voltage indicates an upward bending of the energy band, suggesting an internal potential barrier at the surface. When the applied voltage is 250 V, a FES peak appears. The field-emission electron energy at the UPS and FE peak positions is VL, suggesting that electrons pass from the conduction band through the NEA surface and are then emitted. The peak position of FES shifts to the low-energy side, indicating a reduction in the internal potential barrier, signifying that the external electric field reduces the internal potential barrier height and promotes FE.[71]

Undoped polycrystalline diamond (PCD) particles with sharp edges display electron emission at relatively low turn-on fields (0.8–2.0 $V\cdot\mu m^{-1}$), while no emission is detected for their single-crystal counterparts (Fig. 5(c)). This implies that carrier transport in undoped PDP could potentially take place through grain boundaries within the particles.[81] Defects in diamond can decrease the turn-on field for electron emission, suggesting that pure-phase or single-crystal diamond may not necessarily outperform mixed-phase diamond emitters.[86] P-type diamond exhibits low-threshold FE properties,[71] but the emission of electrons from the p-type diamond NEA surface necessitates a higher electric field.[87] The addition of nitrogen to CH_4/H_2 plasma has been reported to enhance the formation of nanographite phases in grain boundaries. This effectively reduces the size of diamond grains from micron to nanoscale, thereby improving film conductivity and FE performance.[88] On the one hand, the grain boundary conduction improves the FE performance of N-doped NCD films, but on the other hand, the insulating NCD diamond grains restrict the conduction at grain boundaries. In single-crystal diamond and PCD, P can act as a donor and be integrated into different positions within the grains and can be directly doped into the diamond lattice, making the diamond grains conductive.[89] N-type P-doped diamond contains electrons situated in the conduction band and is also anticipated to emit electrons.[71] However, observing electron emission at low threshold voltage/field using P-doped PCD films is indeed challenging, although relatively low field-emission threshold was achieved for heavily P-doped diamond films.[33]

The P and N co-doping is proposed to produce NCD films and results in the acquisition of a large quantity of diamond grains with conductive grain boundaries under varying N_2 concentrations.[82] Figure 5(d) illustrates that with an increase in N_2 content, *E* decreases sharply, while the current density shows a significant rise. In addition, at a N_2 ratio of 0.5%, the electric field that the film can activate reduces by half, which

is presumed to be linked to the film's broader grain boundaries. Conductive atomic force microscopy (C-AFM) analysis has shown that the intensity of the contrast in the images corresponds to the magnitude of the emission current, with a notably higher emission current observed at the grain boundaries of the sample. Electrons in diamond films exhibit a preference for utilizing the grain boundaries as a pathway to ascend from the bottom of the film to the surface, where they are subsequently emitted.[90] When the particles are conductive, they facilitate the transportation of current through themselves and subsequent emission from the crystal faces. Therefore, the presence of a high density of localized electron emission sites in the NCD, indicative of the formation of conductive nanochannels at the grains and grain boundaries, consequently leads to enhanced field-emission efficiency.[91] The nickel (Ni) ion implantation process can also change the EF performance and surface morphology of NCD films, forming a "pine forest" phase sp^2 C=C bond, thereby improving the EF performance. In addition, the Ni injected into the film surface forms a uniform network structure and rich nanographitic phase, becoming a new extremely conductive channel. These channels induce significant electron emission from the film surface, thus bringing excellent conductivity and enhanced EF performance to the Ni-doped film (Fig. 5(e)).[83] In addition, the FE of diamonds can not only decrease the required electric field for activation through doping, but also be controlled to turn on and off, and the intensity of current can be extracted as desired by exposure to light.[72] Figure 5(f) shows that when the H-terminated conductive diamond surface is illuminated by visible light at RT, the field-emission intensity increases by an order of magnitude with increasing illumination intensity until a specific photon flux is reached. This phenomenon implies that the emitted light is not simple, as it consists of low-energy photons well below the diamond band gap, and the emission is insensitive to the photon energy. Nonetheless, regardless of the exact mechanism of triggered field electron emission in diamond under illumination, the observed enhancement of field emission under illumination offers a straightforward means to rapidly modulate the emission current, thereby opening up a wide range of potential applications.[72]

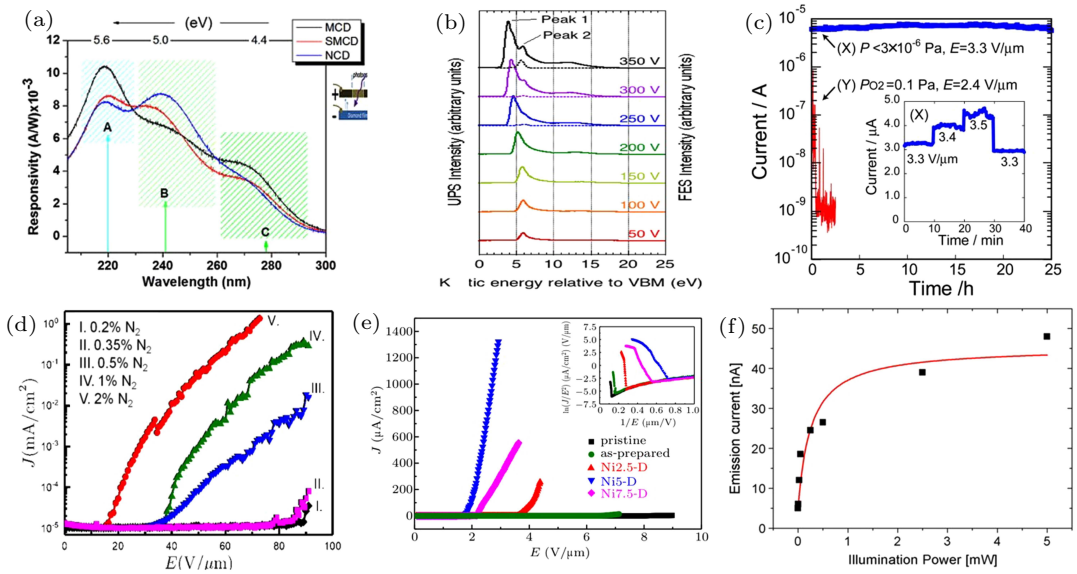


Fig. 5. (a) Spectrum of sulfur-doped diamond in 200–300 nm.[80] (b) Ultraviolet photoelectron and FE spectra of P-doped H-terminated diamond under different applied voltages.[71] (c) PDP FE current versus time. Inset is the current response to the electric field during sample operation.[81] (d) Fowler–Nordheim diagram of FE current density as a function of applied field and the corresponding *J*–*E* characteristic curve.[82] (e) FE characteristics of nickel-doped diamond films.[83] (f) Photoelectric FE current of illumination power (green light) at a fixed voltage with 800 V.[72]

3.2. Photo-induced electron emission

Photoelectron emission (PE) is a surface-dominant process in traditional semiconductor materials. Figure 6(a) illustrates the schematic diagram of the process of PE.[92] The relative intensity of the electron emission peak changed noticeably with the particular photon energy in comparison to the highest emission at the Fermi level. The energy roughly corresponds to the photon energy. The photoelectrons are excited from states near the Fermi level, and the discrepancy between the emission peak and the excitation energy suggests that the scattering process impacts the emission. Optical transitions in diamond occur through the absorption of photons along with phonon absorption or emission. On surfaces with NEA, optically excited electrons in the conduction band of the bulk material can diffuse to the surface and be emitted with minimal hindrance.[93,94] For example, photoelectrons are excited from near the Fermi level, while under the same experimental conditions, no PE was observed on the bare molybdenum substrate, indicating that the electron emission originates from the diamond.[92]

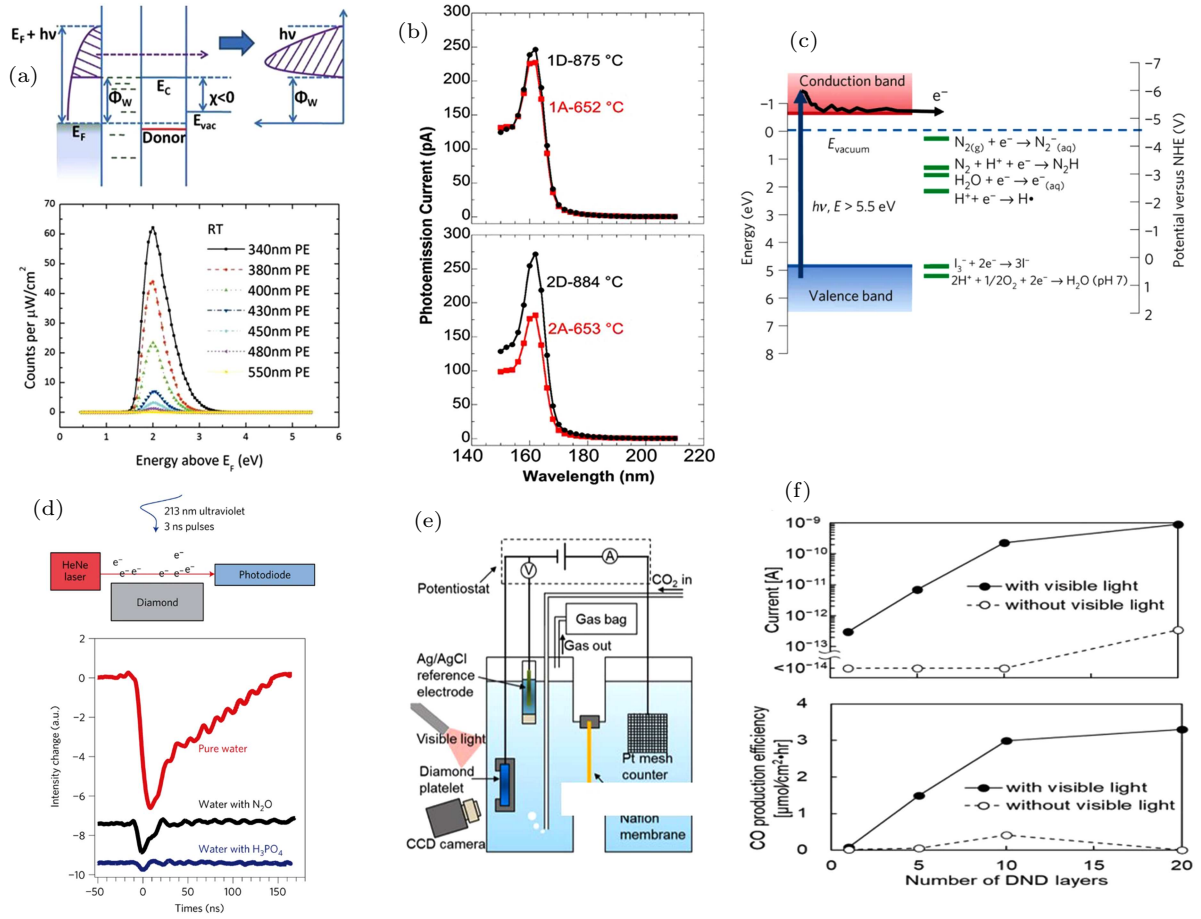


Fig. 6. (a) Schematic diagram of PE and PE spectrum (normalized) of N-doped diamond at ambient temperature.[92] (b) PE current of films without a buffer layer and with a buffer layer obtained at different deposition temperatures.[95] (c) Electronic energy-level diagram of diamond and detection of solvated electrons generated by light excitation in water (d).[96] (e) Schematic diagram of a quartz electrochemical cell measuring the catalytic performance of diamond sheets and (f) electron emission current of diamond sheet and production efficiency of $CO_2 \rightarrow$CO reduction reaction (visible light and dark).[97]

Diamond films with and without a diamond buffer layer (BL) were fabricated at various deposition temperatures.[95] The sample grown at the highest deposition temperature exhibited the highest PE current (Fig. 6(b)). PE and TE properties of the sample were improved by the presence of the buffer layer, which dictates the single-grain morphology and low surface roughness.

In addition, the emission performance is influenced by the deposition temperature since it impacts the shape and size of the grains. The volume fraction of the grain boundaries and the incorporated hydrogen will induce variations in the surface electron affinity. Diamond films grown at higher deposition temperatures were found to have a higher hydrogen content, resulting in smaller grain size and more grain boundaries. The higher hydrogen content leads to a very low NEA, thereby facilitating the efficient escape of photo and thermally generated electrons.

The release of electrons from diamond into a vacuum has been extensively researched, but the ejection of electrons into a liquid has remained largely unexplored. Previous studies have proposed that stimulating diamond with intense laser pulses nearing 100 mJ could cause the photoreduction of water and graphene oxide.[98] When the H-terminated diamond surface is exposed to light with energy of $h\nu > 5.5$ eV, excited electrons can move to the surface and be emitted directly into the vacuum with minimal potential barriers, making diamond a solid-state electron source.[99] This characteristic enables diamonds to release electrons (a highly effective reducing agent) directly into the solution without requiring the transportation of the reactants to an electron source.[10] Exposing H-terminated diamond to light causes the injection of electrons into the reactive liquid, demonstrating the potential application of conventional continuous light sources as photocatalysts.[101] In Figs. 6(c) and 6(d), the emission of electrons from diamond into water can create a solvation electron pool, which can trigger high-energy reduction reactions, such as reducing H^+ to H·, which subsequently reacts with N_2 to form N_2H and ultimately NH_3. The most direct way to detect electron emission from diamond into water is to monitor the resulting solvated electrons.[96] A pulsed UV laser is utilized to irradiate the sample, where the intensity of the transmitted 632 nm light rapidly decreases. Subsequently, as the solvated electrons undergo recombination and other reactions, the intensity returns to its original value with a decay time of ap-

proximately 92 ns. With the addition of a small quantity of phosphoric acid, there is a decrease in pH value, the duration of the temporary signal diminishes, and the temporary absorption signal nearly vanishes under acidic conditions (pH 2).[96]

Diamond films were grown on niobium metal substrates. Although the initial electron yields of the samples were similar, the lifetime of the solvated electrons significantly decreased.[102] Silver nanoparticles impact the photocatalytic properties of diamond. The diamond film contains metal nano-silver particles, and both above and below, the diamond bandgap energy was heightened. This increased absorption and scattering amplifies the diamond's capacity to release electrons and trigger electron-induced reduction of nitrogen to NH_3.[103] Furthermore, as depicted in Fig. 6(e), heavily N-doped diamond sheets were fabricated. The electrons emitted upon deep ultraviolet light excitation traversed the H-terminated diamond surface, entered the CO_2-saturated aqueous solution, and effectively catalyzed the reduction of CO_2 to CO.[97] These results emphasize the substantial potential of H-terminated diamond with high reducing capability in solid-state electron source applications. The efficiency of diamond as a solid-state electrochemical reducing agent can be improved by enabling diamond to absorb visible light or by utilizing diamond samples with various doping (Fig. 6(f)).[97,104]

3.3. Thermal-induced electron emission

3.3.1. Thermionic emission

Thermionic emission (TE) necessitates heating the material within a vacuum to the temperature at which electrons can be emitted, ensuring that the electrons acquire sufficient kinetic energy to escape from the surface. This method efficiently generates electricity by directly converting heat into electrical energy without the use of moving parts (Fig. 7).[106] However, the high operating temperatures limit its application in professional fields, such as communication traveling wave tubes, space thrusters and scientific instruments. It is possible to obtain thermionic emission at low temperatures because the minimum value of the diamond conduction band is higher than the vacuum electron energy.[107]

The NEA property of diamond counteracts the potential barrier due to band bending, enabling electrons to pass through the barrier with sufficient energy input.[25] By optimizing the material parameters of the electron emitter and collector, it is possible to achieve conversion efficiencies approaching those of the Carnot cycle. These parameters can be defined by the Richardson–Dushman law, which quantifies the material's ability to release electron current at a specific temperature as a function of the emission barrier or work function and the emission or Richardson constant. In summary, the emission current of metal depends on the material parameters, work function (Φ) and emission parameter (A_R).[45] The Richardson–Dushman equation theoretically summarizes the direct relationship between the electron emission current density $J(T)$ and the material parameters

$$J(T) = A_R T^2 \, e^{\frac{\Phi}{k_B T}}, \tag{1}$$

where J represents the emission current density, T is the absolute temperature of the emitting material, k_B is Boltzmann's constant and A_R is Richardson's constant.[45] The Φ plays a crucial role in emission. For most metals with a Φ of approximately 5 eV, the minimum temperature required to achieve a usable electron current density (> 1 A·cm^{-2}) in the device is generally higher than 1500 °C. This is challenging to attain in practical applications and necessitates high energy requirements.

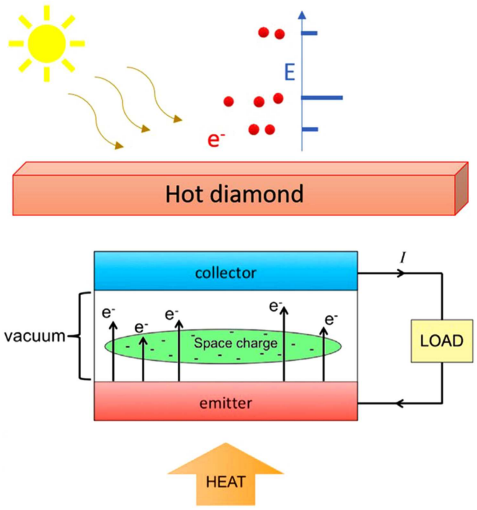


Fig. 7. Simplified diagram of the TE process.[16,105]

The NEA surface of diamond is essential for TE, while electron affinity of the diamond surface typically ranges around -1.1 eV.[108] The H-terminated diamond can generate thermionic current, enabling material stability and efficient device operation even at low temperature.[109,110] Effective thermionic converters can be realized using doped-optimized diamond electrodes, and operating at elevated temperatures can mitigate the Schottky barrier at the diamond collector contacts. Although P doping does not alter the surface state, it can reduce the space charge width of the band-curved surface and enhance hot electron emission performance through heavy doping. The secondary ion mass spectroscopy (SIMS) demonstrates even distribution of P atoms in the film, with a maximum doping concentration of 5×10^{20} cm^{-3}, which serves as the cathode material for thermionic emission.[111] Figure 8(a) depicts that the TE begins at approximately 2 V under different temperature conditions and saturates at around 6 V. The saturation current density increases with rising cathode temperature, reaching a maximum current density at 600 °C. Furthermore, TE current is only observed on the H-terminated

surface, and the emission repeatability is confirmed within the specified temperature range.

Kataoka *et al*. introduced a configuration with layers of low-resistance P-doped and N-doped diamond in a stacked emission structure.[112] The *I*–*V* shows that the current densities were nearly identical in different electrode areas across the entire temperature range, indicating uniform current distribution under the electrode. With the temperature increasing to 873 K, P-doped and stacked films exhibit notably lower resistance compared to N-doped films. In the thermal electron-emission *I*–*V* curves, the high work function of the metal within a specific temperature range leads to electron emission from the opposing metal electrode being negligible, indicating that the emission current likely originates from TE from the diamond emitter. The current increases with voltage and tends to saturate at 8 V, and significantly increases in the stacked structure, demonstrating the significant enhancement of TE in the stacked structure.

The P and N implanted diamond was fabricated on molybdenum substrates,[113] and the N-doped diamond film showed a significant increase in the emission current density, as depicted in Figs. 8(b) and 8(c), with the Richardson constant reaching approximately 10.7 $A{\cdot}cm^{-2}{\cdot}K^2$. Subsequent vacuum emission indicated that the introduction of methane led to a significant increase in current, attributed to the ionization process resulting from resonant electron capture, establishing transient negative ions, and enhancing charge transfer at the emitter surface. The introduction of methane also led to a significant increase in power output, coupled with a shift in maximum power towards lower load resistance, demonstrating that space charge mitigates the ionization process of gaseous species.[113] Introducing low-resistivity N doping into the ultra-NCD interstitial layer can regulate the resistivity of the diamond emitter.[108] 90–100 nm NCD film doped with B was grown on a heavily doped p-type silicon substrate, which preferred structural characteristics, comparatively low internal resistance, and the electrons can be emitted directly from sp^2 bonds, facilitating electron transport to the sp^3 electron emission site. In Fig. 8(d), it was observed that using the concentrated light source resulted in an approximately 80-fold increase at 600 °C, indicating enhanced thermionic emission due to sunlight absorption. Furthermore, when the temperature exceeds 600 °C, the impact of photons in enhancing the thermionic emission mechanism begins to diminish, with it transitioning to a pure thermionic emission state.[114]

The metal substrate reduces the overall emitter resistivity, resulting in a notable rise in emission current density. Refractory metals, such as molybdenum and tungsten, are widely utilized in thermionic emitter devices for forming interfacial layers. In the carbon-rich environment where diamond is grown, these interstitial layers might become unstable due to increased resistivity and decreased Richardson constant, limiting emission current density. A rhenium interstitial layer that does not form carbides and has low carbon solubility can enhance the thermionic emission of nitrogen-doped diamond emitters.[108] The electron emission of PDD samples grown on water-cooled molybdenum substrates under sub-bandgap illumination on diamond was confirmed to have been enhanced (Fig. 8(e)).[105]

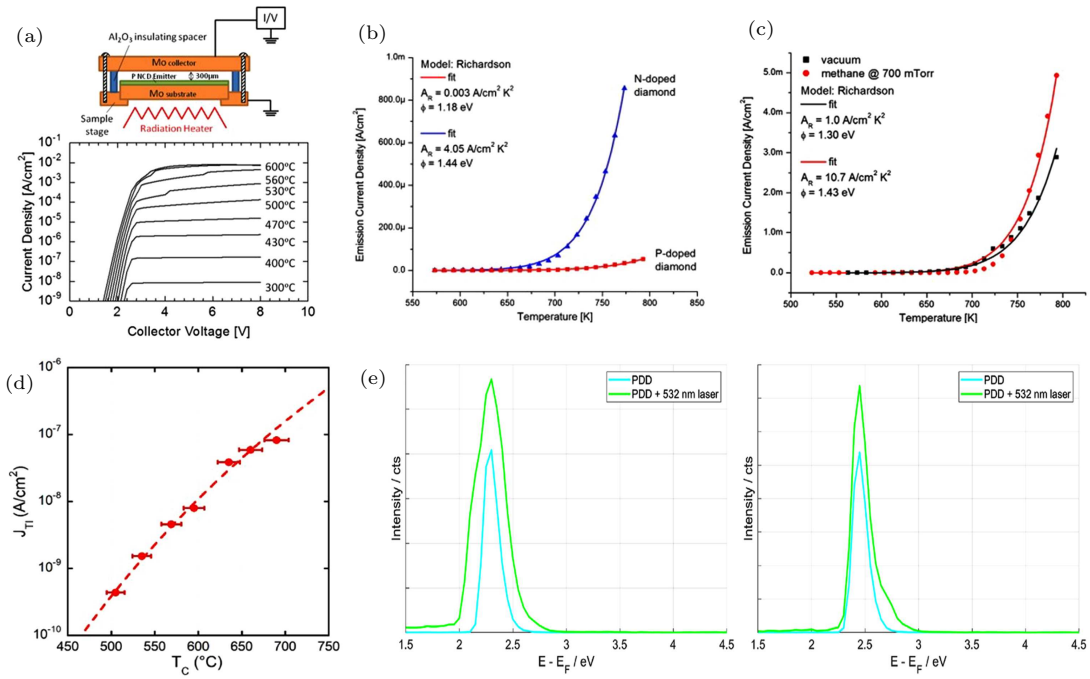


Fig. 8. (a) TE characteristics at operating temperatures from 300 °C to 600 °C.[111] Typical P, N-doped diamond film fitted by Richardson–Dushman (b) and (c).[113] (d) TE spectrum of the NCD film.[114] (e) TE spectra of hydrogen-sealed PDD surfaces under laser irradiation at 300 °C and 400 °C at 532 nm.[105]

3.3.2. Photon-enhanced thermionic emission

A new concept, as shown in Fig. 9, where photon-enhanced thermionic emission (PETE) has also been recently proposed, combines the advantages of photoexcitation and TE processes.[116] It consists of two parallel plates — an electron emitter and a collector — separated by a vacuum gap, and sunlight illuminates the emitter to induce PETE. The p-type semiconductor used combines the advantages of photovoltaics and hot electrons, using photoinduced quasi-Fermi level splitting to reduce the effective electron emission barrier while providing high output voltage. It also utilizes the thermalization process to help electrons escape from the material.[17,115]

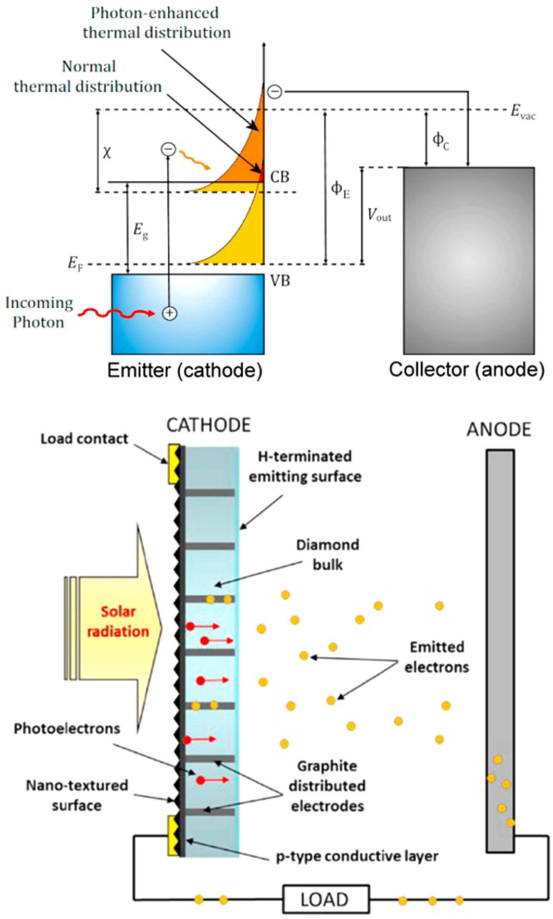


Fig. 9. Schematic diagram of PETE.[17,115]

The PETE occurrence process is divided into three simple steps: first, the electrons in the PETE cathode are excited by solar radiation and enter the conduction band; second, they are rapidly heated to equilibrium heat distribution in the conduction band according to the temperature of the material and diffuse to the entire cathode; thirdly, electrons from the surface with energy greater than the electron affinity are emitted directly into the vacuum and collected at the anode, thus producing an electric current. Therefore, each emitted electron collects photon energy to overcome the material band gap and thermal energy to overcome the material's electron affinity. Due to this "thermal boost", the total voltage generated can be higher than that of photovoltaic power generation with the same band gap, making fuller use of the solar source. Diamond's NEA surface significantly contributes to PETE efficiency.[115,117]

The investigation focused on the visible sub-bandgap PE of PCD films. It was observed that the substrate material and diamond film thickness did not significantly impact the PE yield. However, the nitrogen doping level and grain size had a strong effect on the PE yield. In comparison to MCD films, NCD films exhibited lower electron emission yields due to the high number of defects present in them, which trap excited electrons before they can escape into the vacuum, thereby limiting electron emission. The activation energy of the trap level was determined using the Richardson–Dushman equation. According to the PETE model (the colored dotted line part of Fig. 10(a)), the low activation energy of the trap level enables trapped electrons to be thermally excited back to the CBM at high temperatures, thereby increasing the overall electron emission yield. This process is significant only under low injection conditions, where the cooperativity of photoelectrons is below the trap-level density, and is negligible under high injection conditions.[118]

PETE has the potential to greatly increase the intensity of hot electron emission in p-type semiconductors, with increasing temperature, and the emission intensity increases by almost one order of magnitude (Fig. 10(b)).[119] The undoped hydrogenated PCD were exposed to different monochromatic wavelengths at temperatures between 298 K and 873 K, and kept track of the intensity of electron emission in relation to temperature. The results obtained were also compared with the TE of the same sample measured in the absence of light. Due to the decrease in electron diffusion length with decreasing temperature, the thermionic emission of all wavelengths decreases as the temperature increases. Note that the PEEM is contingent upon the wavelength of the incident light and is more prominent at shorter wavelengths. The rise in photocurrent with temperature aligns with the Richardson–Dushman equation.[117] The emission intensity increases with rising photon energy at low temperatures, aligning with expectations of photoelectric emission. Importantly, the strength of diamond on silicon substrates notably increases with temperature, while the strength of diamond on metal substrates remains relatively constant. The PETE mechanism is consistent with the heightened emission intensity of diamond films on Si substrates. The generation and transmission of photoelectrons may involve a complex process, potentially occurring in the substrate, a nucleation layer with higher sp^2 bond density at grain boundaries or be associated with lower energy in the Si substrate due to reduced photon absorption.[92]

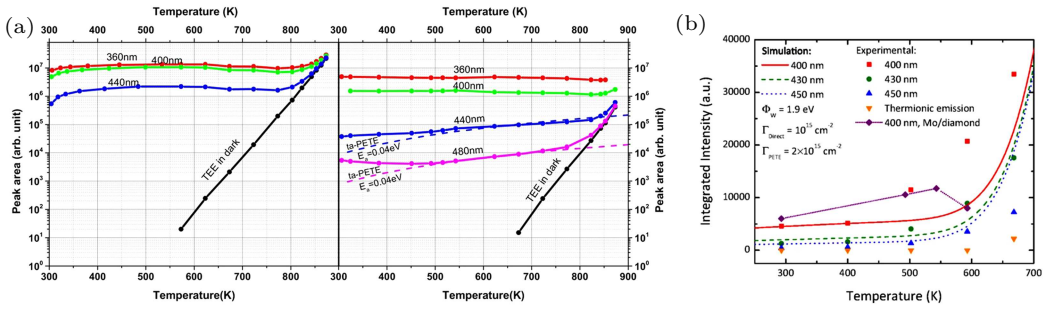


Fig. 10. (a) Thermal electron and PE spectra of N-doped diamond films.[118] (b) Temperature dependence of PE spectrum intensity and TE intensity of N-doped diamond on Si substrate.[119]

4. Summary and outlook

In summary, although diamond has excellent overall electrical and thermal properties, its atomic radius and lattice constant are small, and its band gap is large, which makes the solubility of many impurity atoms in diamond very low, making it difficult for doping, especially n-type doping. N-type diamond forms the basis for the implementation of numerous electron-emitting devices, and further research and production testing are essential for developing viable and efficient diamond PN junction electron-emitting devices. Diamond is essentially insulating, leading to unsatisfactory field-emission performance of existing diamond devices. The protruding tips can concentrate the energy of the device and reduce the excitation field strength. The diamond photon-enhanced thermal ion energy converter combines photo-induced and thermally induced electron emission, which maximizes the energy conversion of power, thereby overcoming the limitations of the two technologies. The H-diamond surface has a low electron affinity, which can maintain stability at relatively high operating temperatures. Therefore, the surface of NEA diamond is commonly used as the emission layer of electron emitters in experiments.

Accordingly, prospective views and research directions for further improving the performance of diamond and expanding its application scope are proposed.

1. While numerous techniques have been investigated for achieving highly doped n-type diamond, only a few have proven successful. At present, it is feasible to manufacture device-compliant B-doped p-type PCD films. The manufacture of high-quality n-type diamond films continues to pose significant challenges, thereby severely restricting the use of diamond in the semiconductor microelectronics industry.

2. During chemical vapor deposition growth, impurities tend to preferentially occupy the amorphous carbon grain boundary positions, leading to undoped grains. To address this issue, an ion injection method can be employed to dope the nanodiamond film with P or oxygen ions to uniformly dope the impurities within the grains. The p-type semiconductor nature of diamond generally results from the hydrogen-rich environment during the growth process. If other elements, such as oxygen, are present in the annealing atmosphere, the H-terminated nanodiamonds can be transformed into oxygen-terminated nanodiamonds, and the p-type semiconductors can be transformed into n-type semiconductors. Domestic research teams have conducted initial studies, and further extensive experimental work is required to validate the potential application of n-type diamond functionalization.

3. The appropriate amount of chemical doping can enhance the physical properties of the device, and highly crystalline diamond films can provide good electronic pathways. However, additional doping gas sources and manufacturing processes make the manufacturing process more complex. Scientists should further explore cost-saving production processes and reduce the use of toxic and harmful gases and precious metals.

Diamond in electron emitter devices has enormous potential, and there will be more new technologies in the future to improve the production and emission performance of diamond films. However, the associated costs and structural complexity may pose significant challenges to the commercial viability of the launcher. In addition to investigation into the quality of intrinsic and doped diamond films, there still exists a large gap between the expected emission performance of diamond films and reality. In the future, in the study of theoretical growth/electron emission mechanisms, it is necessary to further understand and control the adjustment of the surface morphology, work function and conductivity of NEA to realize better high-performance diamond electron emitter devices.

Acknowledgements

This work was supported by the National Natural Science Foundation of China (Grant No. 62274084) and the Fundamental Research Funds for the Central Universities (Grant No. 0210-14380193).

References

[1] Mahmood N, Mehmood M Q and Tahir F A 2020 *Sci. Rep.* **10** 18502
[2] Jhong Y S, Tseng H T and Lin S J 2019 *J. Alloys Compd.* **801** 589
[3] Bunkin N, Shkirin A, Babenko V, Sychev A, Lomkova A and Kulikov E 2015 *Phys. Wave Phenom.* **23** 161

[4] Mallik A K, Dandapat N, Chakraborty S, Mandal A K, Ghosh J, Unnikrishnan M, Bysakh S and Balla V K 2014 *Process. Appl. Ceram.* **8** 69

[5] Yang N J, Yu S Y, Macpherson J V, Einaga Y, Zhao H Y, Zhao G H, Swain G M and Jiang X 2019 *Chem. Soc. Rev.* **48** 157

[6] Tang H, Yuan X H, Cheng Y, Fei H Z, Liu F Y, Liang T, Zeng Z D, Ishii T, Wang M S and Katsura T 2021 *Nature* **599** 605

[7] Wan L F, Mu C Y, Liu Y F, Cheng S H, Wang Q L, Li L A, Li H D and Zou G T 2022 *Chin. Phys. Lett.* **39** 036801

[8] Mallik A K, Shivashankar S A and Biswas S K 2009 *Sadhana* **34** 811

[9] Crawford K G, Maini I, Macdonald D A and Moran D A 2021 *Prog. Surf. Sci.* **96** 100613

[10] Makino T, Oyama K, Kato H, Takeuchi D, Ogura M, Okushi H and Yamasaki S 2014 *Jpn. J. Appl. Phys.* **53** 05FA12

[11] Wen B, Zhao J J and Li T J 2013 *Int. Mater. Rev.* **52** 131

[12] Okano K, Yamada T, Sawabe A, Koizumi S, Itoh J and Amaratunga G A J 2001 *Appl. Phys. Lett.* **79** 275

[13] Kageura T, Hideko M, Tsuyuzaki I, Morishita A, Kawano A, Sasama Y, Yamaguchi T, Takano Y, Tachiki M, Ooi S, Hirata K, Arisawa S and Kawarada H 2019 *Sci. Rep.* **9** 15214

[14] Aharonovich I, Greentree A D and Prawer S 2011 *Nat. Photonics* **5** 397

[15] Gao J, Niu J J, Qin S and Wu X 2017 *Sci. China: Earth Sci.* **60** 207

[16] James M C, Fogarty F, Zulkharnay R, Fox N A and May P W 2021 *Carbon* **171** 532

[17] Sankaran K J, Yeh C J, Drijkoningen S, Pobedinskas P, Van Bael M K, Leou K C, Lin I N and Haenen K 2016 *Nanotechnology* **28** 065701

[18] Sankaran K J, Ficek M, Kunuku S, Panda K, Yeh C J, Park J Y, Sawczak M, Michałowski P P, Leou K C and Bogdanowicz R 2018 *Nanoscale* **10** 1345

[19] Shimaoka T, Kuwabara D, Hara A, Makino T, Tanaka M and Koizumi S 2017 *Appl. Phys. Lett.* **110** 212104

[20] Yang H C, Ma Y D and Dai Y 2022 *Functional Diamond* **1** 150

[21] Raymakers J, Haenen K and Maes W 2019 *J. Mater. Chem. C* **7** 10134

[22] Sun T, Koeck F A, Rezikyan A, Treacy M M and Nemanich R J 2014 *Phys. Rev. B* **90** 121302

[23] Salvatori S, Brugnoli E, Rossi M C and Pinzari F 2001 *Diamond Relat. Mater.* **10** 852

[24] Masuzawa T, Shiraki Y, Kudo Y, Saito I, Yamaguchi H, Yamada T and Okano K 2008 *Appl. Surf. Sci.* **254** 6285

[25] Takeuchi D, Ogura M, Ri S G, Kato H, Okushi H and Yamasaki S 2008 *Diamond Relat. Mater.* **17** 986

[26] Salerno R, Valentini V, Bolli E, Mastellone M, Serpente V, Mezzi A, Tortora L, Colantoni E, Bellucci A and Polini R 2024 *ACS Appl. Energy Mater.* **7** 868

[27] Donato N, Rouger N, Pernot J, Longobardi G and Udrea F 2019 *J. Phys. D: Appl. Phys.* **53** 093001

[28] Ikeda T and Teii K 2009 *Appl. Phys. Lett.* **94** 14

[29] Yamada T, Masuzawa T, Mimura H and Okano K 2016 *J. Phys. D: Appl. Phys.* **49** 045102

[30] Takeuchi D, Makino T, Kato H, Okushi H and Yamasaki S 2011 *Physica Status Solidi (a)* **208** 2073 2073

[31] Geis M W, Efremow N N, Krohn K E, Twichell J C, Lyszczarz T M, Kalish R, Greer J A and Tabat M D 1998 *Nature* **393** 431

[32] Sugino T, Kuriyama K, Kimura C, Yokota Y, Kawasaki S and Shirafuji J 1999 *J. Appl. Phys.* **86** 4635

[33] Yamada T, Nebel C E, Rezek B, Takeuchi D, Fujimori N, Namba A, Nishibayashi Y, Yamaguchi H, Saito I and Okano K 2005 *Appl. Phys. Lett.* **87** 234107

[34] Yamada T, Nebel C E, Somu K, Uetsuka H, Yamaguchi H, Kudo Y, Okano K and Shikata S I 2007 *Physica Status Solidi (a)* **204** 2957

[35] Lloret F, Sankaran K J, Millan-Barba J, Desta D, Rouzbahani R, Pobedinskas P, Gutierrez M, Boyen H G and Haenen K 2020 *Nanomaterials (Basel)* **10** 1024

[36] Sankaran K J, Chen H C, Sundaravel B, Lee C Y, Tai N H and Lin I N 2013 *Appl. Phys. Lett.* **102** 061604

[37] Kachwala A, Chubenko O, Kim D, Simakov E and Karkare S 2022 *J. Appl. Phys.* **132** 224901

[38] Johnson S, Markwitz A, Rudolphi M, Baumann H, Oei S P, Teo K B K and Milne W I 2004 *Appl. Phys. Lett.* **85** 3277

[39] Nagao M, Tamura Y, Matsukawa T, Kanemaru S, Itoh J and Tokunaga K 2002 *J. Vac. Sci. Technol. B* **20** 2309

[40] Lenk C, Lenk S, Holz M, Guliyev E, Hofmann M, Ivanov T, Rangelow I W, Behzadirad M, Rishinaramangalam A K, Feezell D and Busani T 2018 *J. Vac. Sci. Technol. B* **36** 06

[41] Lu X, Yang Q, Chen W, Xiao C and Hirose A 2006 *J. Vac. Sci. Technol. B* **24** 2575

[42] Torresin O, Borz M, Mauchain J, Blum I, Kleshch V I, Obraztsov A N, Vella A and Chalopin B 2019 *Ultramicroscopy* **202** 51

[43] Ramaneti R, Sankaran K J, Korneychuk S, Yeh C J, Degutis G, Leou K C, Verbeeck J, Van Bael M K, Lin I N and Haenen K 2017 *APL Mater.* **5** 066102

[44] Chang T H, Kunuku S, Hong Y J, Leou K C, Yew T R, Tai N H and Lin I N 2014 *ACS Appl. Mater. Interfaces* **6** 11589

[45] Lin W, Wang T T, Wang Q L, Lv X Y, Li G Z, Li L A, Ao J P and Zou G T 2022 *Chin. Phys. B* **31** 108105

[46] Zhu Y, Lin W, Li D S, Li L A, Lv X Y, Wang Q L and Zou G T 2023 *Chin. Phys. B* **32** 088101

[47] Koizumi S, Watanabe K, Hasegawa M and Kanda H 2001 *Science* **292** 1899

[48] Takeuchi D, Makino T, Kato H, Hirabayashi I, Okushi H and Yamasaki S 2010 *Physica Status Solidi A* **207** 2093

[49] Lin I N, Koizumi S, Yater J and Koeck F 2014 *MRS Bull.* **39** 533

[50] Shimaoka T, Umezawa H, Ichikawa K, Pernot J and Koizumi S 2020 *Appl. Phys. Lett.* **117** 103902

[51] Takeuchi D, Makino T, Ri S G, Tokuda N, Kato H, Ogura M, Okushi H and Yamasaki S 2008 *Appl. Phys. Express* **1** 015004

[52] Kato H, Makino T, Yamasaki S and Okushi H 2007 *J. Phys. D: Appl. Phys.* **40** 6189

[53] Makino T, Tokuda N, Kato H, Kanno S, Yamasaki S and Okushi H 2008 *Physica Status Solidi A* **205** 2200

[54] Suzuki M, Sakai T, Makino T, Kato H, Takeuchi D, Ogura M, Okushi H and Yamasaki S 2013 *Physica Status Solidi (a)* **210** 2035

[55] Makino T, Yoshino K, Sakai N, Uchida K, Koizumi S, Kato H, Takeuchi D, Ogura M, Oyama K, Matsumoto T, Okushi H and Yamasaki S 2011 *Appl. Phys. Lett.* **99** 061110

[56] Makino T, Ri S G, Tokuda N, Kato H, Yamasaki S and Okushi H 2009 *Diamond Relat. Mater.* **18** 764

[57] Malakoutian M, Benipal M, Koeck F A, Nemanich R J and Chowdhury S 2020 *IEEE J. Electron Devices Soc.* **8** 614

[58] Lobaev M A, Radishev D B, Bogdanov S A, Vikharev A L, Gorbachev A M, Isaev V A, Kraev S A, Okhapkin A I, Arhipova E A, Drozdov M N and Shashkin V I 2020 *Physica Status Solidi RRL* **14** 2000347

[59] Kato H, Ogura M, Makino T, Takeuchi D and Yamasaki S 2016 *Appl. Phys. Lett.* **109** 142102

[60] Oyama K, Ri S G, Kato H, Ogura M, Makino T, Takeuchi D, Tokuda N, Okushi H and Yamasaki S 2009 *Appl. Phys. Lett.* **94** 152109

[61] Kato H, Makino T, Ogura M, Tokuda N, Okushi H and Yamasaki S 2009 *Appl. Phys. Express* **2** 055502

[62] Takeuchi D, Makino T, Kato H, Okushi H and Yamasaki S 2011 *Physica Status Solidi (a)* **208** 2073

[63] Honbu T, Takeuchi D, Ichikawa K, Ohmagari S, Teraji T, Ogura M, Kato H, Makino T and Shoji I 2021 *Diamond and Relat. Mater.* **117** 108463

[64] Koeck F A, Benipal M and Nemanich R J 2020 *Diamond Relat. Mater.* **101** 107607

[65] Okushi H, Watanabe H, Yamasaki S and Kanno S 2006 *Physica Status Solidi A* **203** 3226

[66] Hasan M M, Wang C, Pala N and Shur M 2024 *Nanomaterials* **14** 460

[67] Takeuchi D, Koizumi S, Makino T, Kato H, Ogura M, Ohashi H, Okushi H and Yamasaki S 2013 *Physica Status Solidi (a)* **210** 1961

[68] Takeuchi D, Makino T, Kato H, Ogura M, Tokuda N, Oyama K, Matsumoto T, Okushi H and Yamasaki S 2011 *Diamond Relat. Mater.* **20** 917

[69] Trucchi D M and Melosh N A 2017 *MRS Bulletin* **42** 488

[70] Harniman R, May P W and Fox O J L 2017 *Diamond Relat. Mater.* **80** 147

[71] Yamada T, Masuzawa T, Mimura H and Okano K 2015 *J. Phys. D: Appl. Phys.* **49** 045102

[72] Gan L, Cimmino A, Prawer S, Bolker A and Kalish R 2011 *Diamond Relat. Mater.* **20** 1263

[73] Nebel C E, Yang N, Uetsuka H, Yamada T and Watanabe H 2008 *J. Appl. Phys.* **103** 013712

[74] Yamada T, Nebel C E and Shikata S I 2009 *Appl. Surf. Sci.* **256** 1006

[75] Subramanian K, Kang W, Davidson J, Choi B and Howell M 2006 *Diamond Relat. Mater.* **15** 1994

[76] Yamada T, Hwang D S, Vinod P R, Makino T and Fujimori N 2005 *Jpn. J. Appl. Phys.* **44** L385
[77] Strobel P, Riedel M, Ristein J and Ley L 2004 *Nature* **430** 439
[78] Takeuchi D, Makino T, Kato H, Ogura M, Tokuda N, Oyama K, Matsumoto T, Hirabayashi I, Okushi H and Yamasaki S 2010 *Appl. Phys. Express* **3** 041301
[79] Zhang W, Guan L, Wang B, Liu H, Wang J, Hong X, Long J, Wei S, Xiong X and Xiong Y 2022 *J. Alloys Compd.* **928** 167243
[80] Mendoza F, Makarov V, Weiner B R and Morell G 2015 *Appl. Phys. Lett.* **107** 201605
[81] Nose K, Fujita R, Kamiko M and Mitsuda Y 2012 *J. Vac. Sci. Technol. B* **30** 011204
[82] Lloret F, Sankaran K J, Millan-Barba J, Desta D, Rouzbahani R, Pobedinskas P, Gutierrez M, Boyen H G and Haenen K 2020 *Nanomaterials* **10** 1024
[83] Wang Y, Yu S W, Xue Y P, Hei H J, Wu Y X and Shen Y Y 2021 *Chin. Phys. B* **30** 068101
[84] Kozak H, Kromka A, Ukraintsev E, Houdkova J, Ledinsky M, Vaněček M and Rezek B 2009 *Diamond Relat. Mater.* **18** 722
[85] Tiwari A K, Goss J, Briddon P, Wright N G, Horsfall A B, Jones R, Pinto H and Rayson M 2011 *Phys. Rev. B* **84** 245305
[86] Zhu W, Kochanski G, Jin S and Seibles L 1995 *J. Appl. Phys.* **78** 2707
[87] Yamada T, Sawabe A, Koizumi S, Itoh J and Okano K 2000 *Appl. Phys. Lett.* **76** 1297
[88] Cuenca J A, Sankaran K J, Pobedinskas P, Panda K, Lin I N, Porch A, Haenen K and Williams O A 2019 *Carbon* **145** 740
[89] Janssen W, Turner S, Sakr G, Jomard F, Barjon J, Degutis G, Lu Y G, D'Haen J, Hardy A and Bael M V 2014 *Physica Status Solidi RRL* **8** 705
[90] Harniman R L, Fox O J, Janssen W, Drijkoningen S, Haenen K and May P W 2015 *Carbon* **94** 386
[91] Deshmukh S, Sankaran K, Srinivasu K, Korneychuk S, Banerjee D, Barman A, Bhattacharya G, Phase D, Gupta M and Verbeeck J 2018 *Diamond Relat. Mater.* **83** 118
[92] Sun T, Koeck F A M, Zhu C and Nemanich R J 2011 *Appl. Phys. Lett.* **99** 202101
[93] Takeuchi D, Nebel C E and Yamasaki S 2006 *Physica Status Solidi (a)* **203** 3100
[94] Takeuchi D, Nebel C E and Yamasaki S 2006 *J Appl. Phys.* **99** 086102
[95] Cicala G, Magaletti V, Valentini A, Nitti M A, Bellucci A and Trucchi D M 2014 *Appl. Surf. Sci.* **320** 798
[96] Zhu D, Zhang L, Ruther R E and Hamers R J 2013 *Nat. Mater.* **12** 836
[97] Yoshikawa T, Asakawa H, Matsumoto T, Ichikawa K, Kaga A, Yamamoto S, Izumi R, Ohno M, Mahiko T and Mutsuda M 2024 *Carbon* **218** 118689
[98] Jang D M, Myung Y, Im H S, Seo Y S, Cho Y J, Lee C W, Park J, Jee A Y and Lee M 2012 *Chem. Commun.* **48** 696
[99] Zhu D, Zhang L, Ruther R E and Hamers R J 2013 *Nat. Mater.* **12** 836
[100] Buchner F, Kirschbaum T, Venerosy A, Girard H, Arnault J C, Kiendl B, Krueger A, Larsson K, Bande A and Petit T 2022 *Nanoscale* **14** 17188
[101] Nebel C E 2013 *Nat. Mater.* **12** 780
[102] Hamers R, Bandy J, Zhu D and Zhang L 2014 *Faraday Discuss.* **172** 397
[103] Li S, Bandy J A and Hamers R J 2018 *ACS Applied Materials & Interfaces* **10** 5395
[104] Marchal C, Saoudi L, Girard H A, Keller V and Arnault J C 2023 *Adv. Energy Sustainability Res.* **5** 2300260
[105] Wan G, Cattelan M, Croot A, Dominguez-Andrade H, Nicley S S, Haenen K and Fox N A 2021 *Carbon* **185** 376
[106] Shefsiek P 2010 *IEEE T Plasma Sci.* **38** 2041
[107] Bellucci A, Pede B, Mastellone M, Valentini V, Polini R and Trucchi D 2023 *Ceram. Int.* **49** 24351
[108] Koeck F A M and Nemanich R J 2012 *J. Appl. Phys.* **112** 113707
[109] Koeck F A M, Nemanich R J, Lazea A and Haenen K 2009 *Diamond Relat. Mater.* **18** 789
[110] Kataoka M, Zhu C, Koeck F A M and Nemanich R J 2010 *Diamond Relat. Mater.* **19** 110
[111] Kato H, Takeuchi D, Ogura M, Yamada T, Kataoka M, Kimura Y, Sobue S, Nebel C E and Yamasaki S 2016 *Diamond Relat. Mater.* **63** 165
[112] Kataoka M, Morioka N, Kimura Y, Sobue S, Kato H, Takeuchi D and Yamasaki S 2016 *Physica Status Solidi (a)* **213** 2650
[113] Koeck F A M, Nemanich R J, Balasubramaniam Y, Haenen K and Sharp J 2011 *Diamond Relat. Mater.* **20** 1229
[114] Bellucci A, Pede B, Mastellone M, Valentini V, Polini R and Trucchi D M 2023 *Ceram. Int.* **49** 24351
[115] Schwede J W, Bargatin I, Riley D C, Hardin B E, Rosenthal S J, Sun Y, Schmitt F, Pianetta P, Howe R T, Shen Z X and Melosh N A 2010 *Nat. Mater.* **9** 762
[116] Schwede J W, Sarmiento T, Narasimhan V K, Rosenthal S J, Riley D C, Schmitt F, Bargatin I, Sahasrabuddhe K, Howe R T and Harris J S 2013 *Nat. Commun.* **4** 1576
[117] Elfimchev S, Chandran M, Akhvlediani R and Hoffman A 2015 *Physica Status Solidi (a)* **212** 2583
[118] Elfimchev S, Chandran M, Akhvlediani R and Hoffman A 2017 *Appl. Surf. Sci.* **410** 414
[119] Sun T, Koeck F A M, Rezikyan A, Treacy M M J and Nemanich R J 2014 *Phys. Rev. B* **90** 121302